Early Steps of the Intramolecular Signal Transduction in Rhodopsin Explored by Molecular Dynamics Simulations†

Ute F. Röhrig, Leonardo Guidoni, and Ursula Rothlisberger*,‡

Laboratory of Inorganic Chemistry, Swiss Federal Institute of Technology, CH-8093 Zurich, Switzerland

Received April 23, 2002; Revised Manuscript Received June 27, 2002

ABSTRACT: We present molecular dynamics simulations of bovine rhodopsin in a membrane mimetic environment based on the recently refined X-ray structure of the pigment. The interactions between the protonated Schiff base and the protein moiety are explored both with the chromophore in the dark-adapted 11-*cis* and in the photoisomerized *all-trans* form. Comparison of simulations with Glu181 in different protonation states strongly suggests that this loop residue located close to the 11-*cis* bond bears a negative charge. Restrained molecular dynamics simulations also provide evidence that the protein tightly confines the absolute conformation of the retinal around the C12−C13 bond to a positive helicity. 11-*cis* to *all-trans* isomerization leads to an internally strained chromophore, which relaxes after a few nanoseconds by a switching of the ionone ring to an essentially planar *all-trans* conformation. This structural transition of the retinal induces in turn significant conformational changes of the protein backbone, especially in helix VI. Our results suggest a possible molecular mechanism for the early steps of intramolecular signal transduction in a prototypical G-protein-coupled receptor.

G-protein-coupled receptors (GPCRs)[1] are a large class of membrane proteins that constitute the central components of a variety of biological signal transmission pathways. GPCRs are homologous and structurally alike, heptahelical transmembrane (TM) proteins. They are expressed in most animals and represent more than 1% of the human genome (*1*−*3*). The signaling pathways regulated by GPCRs involve a variety of crucial biological functions such as cell proliferation and survival, angiogenesis, and light and odor detection. Because of their key role in various vital processes, these receptors are the target of more than half of the currently approved therapeutic agents (*4*). The elucidation of the molecular mechanisms underlying GPCR function could provide a basis to control and to interfere with biochemical signaling pathways, and thus a large body of research has been dedicated to the characterization of these receptors. Despite this, the molecular details of the signal propagation mechanism are yet largely unknown. Progress has partly been hampered by the fact that for a long time no high-resolution structural data were available.

The recent X-ray structure of bovine rhodopsin at a resolution of 2.8 Å (*5*) has paved the way for an understanding of the structure−function relationships of a prototypical GPCR at the molecular level (*6*, *7*). Rhodopsins are present in the rod cells of the retina and turn on the signaling transmission cascade that leads to vision (*8*−*10*). The structure of rhodopsin is composed of a seven TM helical bundle surrounding the covalently bound chromophore, the protonated Schiff base of retinal (RPSB; see Scheme 1).

Light absorption by the pigment triggers the isomerization of the 11-*cis* to the *all-trans* form of the RPSB (*11*). This reaction occurs with high efficiency (quantum yield 0.67), and the primary photoproduct, photorhodopsin, is formed within a very short time (200 fs). Subsequently, photorhodopsin thermally relaxes within a few picoseconds to a distorted *all-trans* configuration, bathorhodopsin (*12*). On a nanosecond time scale, bathorhodopsin establishes an equilibrium with a blue-shifted intermediate (BSI) before the mixture decays to form lumirhodopsin. Lumirhodopsin is then transformed into metarhodopsin I and subsequently metarhodopsin II, the active conformation for G-protein coupling (*13*).

Whereas the crystallographic data reveal a detailed description of the receptor in the inactive dark state, the conformational changes experienced by the protein during the signaling pathway have remained largely elusive.

Here, we present computational studies of bovine rhodopsin immersed in a membrane mimetic environment (Figure 1a), with the chromophore both in the 11-*cis* and in the *all-trans* form. We address different open issues concerning the structural and dynamical properties of the photoreceptor in the dark state and investigate the isomerization-induced mechanism for signal propagation from the chromophore to the protein.

Specifically, we endeavor to ascertain the protonation state of potentially ionizable residues close to the active site. Several groups have reported that the immediate protein environment and, in particular, the nearby electrostatic field

† This work was supported by ETH research grants.

* To whom correspondence should be addressed. E-mail: uro@inorg.chem.ethz.ch.

‡ Current address: Laboratory of Computational Chemistry and Biochemistry, Swiss Federal Institute of Technology, CH-1015 Lausanne, Switzerland.

[1] Abbreviations: BSI, blue-shifted intermediate; GPCR, G-protein-coupled receptor; MD, molecular dynamics; RMSD, root mean square displacement; RPSB, retinal-protonated Schiff base; TM, transmembrane.

10.1021/bi026011h CCC: $22.00
Published on Web 07/30/2002

Scheme 1: Retinal-Protonated Schiff Base[a]

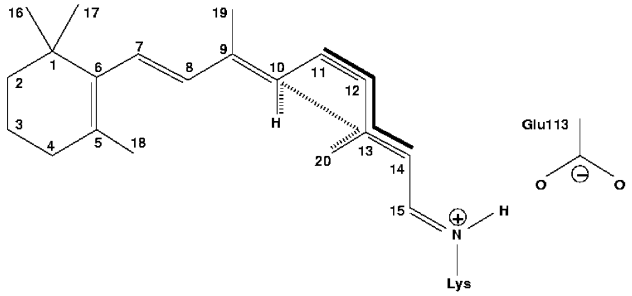

[a] The two dihedral angles mentioned in the text are indicated by a dashed line ($\varphi_{H-C10-C13-C20}$) and a solid line ($\varphi_{C11-C12-C13-C14}$), respectively.

have a crucial influence on the isomerization process (*14*, *15*). It is therefore essential to probe the effect of possible charge variations in the binding pocket.

The X-ray structure reveals three acidic residues (Glu113, Glu122, and Glu181) in the vicinity of the chromophore. Glu113 acts as a counterion of the positively charged chromophore (*16*, *17*) and is thus likely to adopt an anionic form, while Glu122 has been reported to be protonated (*18*). The third acidic residue (Glu181) is part of the second extracellular loop that covers the chromophore binding pocket. Its side chain is located close to the isomerizing double bond (Figure 1b). To date, there is no direct experimental information about the protonation state of Glu181. Mutation studies suggest a protonated side chain (*19*), whereas vibrational spectra fail to show an appropriate band of a protonated carboxylic acid (*20*, *21*). Two-photon spectroscopy experiments suggest an overall neutral binding site (*22*), while NMR spectroscopic measurements (*23*, *24*) predict a negative charge close to the isomerizing double bond. Here, we address the question of the charge state of Glu181 by static Poisson−Boltzmann calculations as well as by explicit solvent MD simulations.

Another issue with potential implications to the isomerization process is the twist of the chromophore around the C12−C13 bond (numbering given in Scheme 1). The absolute configuration of this conformer in the dark state is relevant because it can be expected to influence the sense of rotation during photoisomerization. Different experimental and theoretical studies provide controversial evidence about the absolute twist around the C12−C13 bond, reporting either a positive (*25*−*27*) or a negative helicity (*24*, *28*, *29*). In our MD simulations, we are able to probe if the X-ray-based model of the binding pocket is able to discriminate conformers with a different sense of the helical twist or if both rotamers are likely to coexist.

With the structural model established in this way, we investigate possibilities for forming the isomerized chromophore within the protein and study possible signal transduction pathways. We have addressed this challenging problem via a series of classical isomerization trials, where the dihedral angle around the 11-*cis* double bond was forced to rotate by 180° in a short time and the subsequent movements of the RPSB chromophore and the protein environment were monitored. The full photocycle of rhodopsin leading to G-protein activation takes place on a millisecond time scale and is therefore beyond the time window of present MD simulations. However, the early intermediates can in principle be observed in explicit solvent simulations.

Anticipating our results, we find that the rather close-fitting shape of the binding pocket enables only few routes for possible structural relaxations and that immediately after isomerization the chromophore is forced into a highly strained configuration. Within a multi-nanosecond simulation, the structurally distorted retinal relaxes to an essentially planar geometry. The geometric strain is mainly released through a swinging motion of the β-ionone ring that is the trigger for structural changes in the surrounding helical bundle. In this way, the initially localized geometric perturbation gets amplified to an increasingly larger scale. The intermediate in which the *all-trans* form of the chromophore has relaxed to a planar, unstrained geometry shares common features with the spectroscopically detected BSI (*30*) and lumirhodopsin states and could thus serve as a putative structural model for these intermediates of the signaling pathway.

METHODS

Structural Models. Our computational models are based on the more recent refinement of the crystal structure of bovine rhodopsin (Protein Data Bank accession code 1HZX, chain A), solved at 2.8 Å resolution (*31*). For the sake of comparison, we have also performed one simulation (RHO1f88) based on the earlier refinement of the same structure (Protein Data Bank accession code 1F88, chain A) (*5*). The missing amino acid residues in the third cytoplasmic loop (236−239) and in the C-terminal tail (328−333) were added using the loop library of the program SYBYL (Tripos Inc., St. Louis, MO), taking care to avoid nonphysical contacts with the rest of the protein. The solvent-exposed ionizable side chains are in their default ionization state as well as the C- and N-termini. Amino acids Asp83 and Glu122 within the protein core are assumed to be neutral as detected by FTIR experiments (*18*). The Schiff base linkage between Lys296 and the chromophore bears a net positive charge compensated by the counterion Glu113 (Figure 1b) (*16*, *17*). All histidine residues present in the protein are assumed to be protonated either in the N_δ position (His100, His211) or in the N_ϵ position (His65, His152, His195, His278). To investigate the protonation state of Glu181, two different models were considered, one with a negatively charged (RHO) and one with a protonated carboxy group (RHOp). In the latter, the proton of the carboxy group is pointing toward the hydroxy group of Tyr268, while the carboxy oxygens are hydrogen bonded to the hydroxy group of Tyr192 and to an internal water molecule. Overall neutral systems at physiological ion concentration (≈150 mmol/L) were obtained by adding sodium and chloride ions to the aqueous phase. Initial positions were obtained by calculating the electrostatic potential around the protein via numerical solution of the Poisson−Boltzmann equation with the Delphi program (*32*, *33*). Heteroatoms included in the crystal structure (Hg^{2+}, Zn^{2+}, sugars, heptane-1,2,3-triol) are not included in the models, except for the chromophore and two palmitic acid residues bound to Cys322 and Cys323. The program Dowser (*34*) was used to locate internal cavities in the protein and to assess their hydrophilicity by means of calculating the interaction energy of a water molecule with the surrounding atoms. A water molecule was placed in a

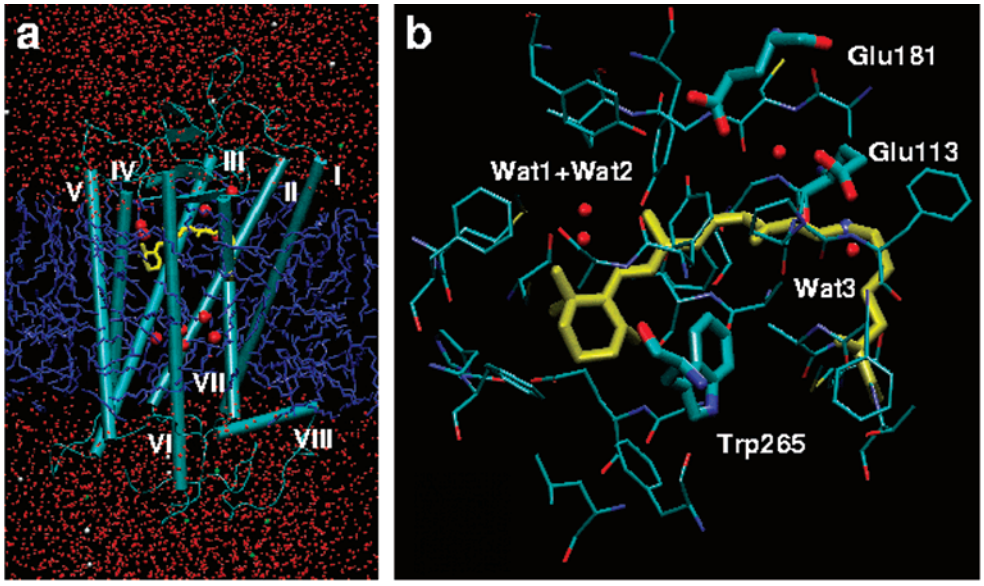

FIGURE 1: (a) Snapshot of the simulated system. Rhodopsin (turquoise) is represented with the extracellular side on top. The retinal chromophore (yellow) is accommodated within the seven TM helices (numbering given in white). The membrane is mimicked by a layer of *n*-octane (blue) surrounded by a saline solution (water, red; sodium ions, green; chloride ions, white). (b) Snapshot of the retinal chromophore and the residues of the binding pocket within 7 Å of the chromophore with the extracellular side on top. The charged residues (Glu113, Glu181), as well as Trp265 and the internal water molecules, are highlighted.

cavity if the interaction energy was stronger than −12 kcal/mol. By this criterion, which has been found to be able to distinguish hydrated from empty cavities (*34*), ten internal water molecules were obtained: five within 6 Å of the chromophore and five in cavities around Asp83 near the cytoplasmic side. The three internal water molecules resolved in the crystal structure 1HZX (residues 2008, 2009, 2014) are closely reproduced by this procedure. The internal water molecules in our model system are also in excellent agreement with the recently resolved water binding sites in the crystal structure 1L9H (*35*). Except for site number 3 (numbering according to ref *35*), all seven sites found in the crystal data were identified in the calculations.

In all models, the cell membrane is mimicked by a 56 × 46 × 30 Å^3 layer of *n*-octane immersed in a box of water of approximately 56 × 46 × 91 Å^3. This approach provides a stable hydrophobic/hydrophilic liquid interface quickly adaptable to the protein structure and has been successfully applied in simulations of helix bundles (*36*, *37*) and of ionic channels (*38*−*40*). The box dimensions are chosen in such a way that the initial minimum gap between periodic images of the protein is 12 Å. The protein was immersed in the box using the intracellular part of helix IV as the axis perpendicular to the membrane plane (*41*) and placing residues 155−173 in the hydrophobic part of the membrane. This results in a model where helix VIII lies at the hydrophobic/hydrophilic interface, with the hydrophilic residues (Lys311, Gln312, Arg314, Asn315, and Thr319) pointing toward the aqueous phase. The total number of atoms in our models is about 24000 (Figure 1a).

Parametrization. The all-atom AMBER force field (*42*) was used for the protein, whereas the OPLS (*43*, *44*) and the TIP3P (*45*) models were used for *n*-octane and water, respectively. The force fields for the retinal chromophore and the palmitic acid residues were developed using the recommended AMBER procedure. The atomic charges were derived by multiconfigurational RESP fitting (*42*, *46*, *47*), using HF/6-31G* optimized structures and electrostatic potentials obtained with the Gaussian 98 program package (*48*). For the chromophore, a model system consisting of the protonated Schiff base of retinal terminated by a propyl tail was considered both in the *all-trans* and in the 11-*cis* conformation. During the RESP fitting, an additional restraint was applied to fix the charge of the terminal methyl group of the propyl tail to the charge of the corresponding part of the lysine residue in the AMBER force field.[2] Standard AMBER torsional parameters were used for the palmitic acid residues, while those obtained by Tajkhorshid et al. (*49*) [parameter set B, obtained from UB3LYP/6-31G* calculated barriers for a protonated model Schiff base (*50*)] were used for the chromophore. All van der Waals parameters were taken from the standard AMBER force field.

Molecular Dynamics Calculations. Simulations at ambient temperature (300 K) and pressure (1 bar) were carried out with the SANDER module of the AMBER 6 package (*51*) using periodic boundary conditions. Electrostatic interactions were calculated with the Ewald particle mesh method (*52*) with a grid spacing of about 1 Å and a spline interpolation of order 4. We used a cutoff of 10 Å for the direct sum part of the Ewald sum and for the Lennard-Jones interactions. Bonds involving hydrogen atoms were constrained using a SHAKE algorithm (*53*). The time integration step was set to 1.5 fs. The system was coupled to a Berendsen bath (*54*) with 0.2 ps relaxation time for the temperature and 1.0 ps for the pressure. The water/*n*-octane box was equilibrated via 0.2 ns of MD. After immersion of the protein and placement of the sodium and chloride ions, the box underwent another 1.0 ns of MD with the protein kept fixed. No phase mixing was observed. The whole system was then energy minimized, restraining the backbone of the protein to the X-ray structure. The system was heated to 300 K

[2] A list of charges and atom types is available as Supporting Information.

during a constant volume MD run of 45 ps. After an additional 45 ps, constant pressure conditions were applied. Data were collected after an equilibration phase of 0.4 ns.

Several MD simulations with varying setups were performed. Throughout the text, we will refer to the different runs via the following labels: RHO1f88 (0.9 ns MD based on 1F88, chain A, with Glu181 unprotonated); RHOp (2.0 ns MD based on 1HZX, chain A, Glu181 protonated); RHO (7.0 ns MD, same setup as RHOp but Glu181 unprotonated); RHOres [1.0 ns MD with the same setup as RHO but restraining the dihedral angle H−C10−C13−C20 (numbering given in Scheme 1) to a value between +40° and +80°]. The force constant of the harmonic restraint was stepwise lowered from 500 (0−270 ps) to 50 (270−405 ps) to 10 (405−540 ps) and to 5 kcal mol^{-1} Å^{-2} (540−675 ps) and released after 675 ps. Furthermore, 24 isomerization trials (16.5 ps each), starting from different snapshots of RHO taken at 90 ps intervals, were carried out. A harmonic potential with a force constant of 50 kcal mol^{-1} Å^{-2} was applied to the C10−C11−C12−C13 torsional angle, changing from −10° to 180° in 1.5 ps. One of the simulations (RHOiso) was extended to a simulation time of 7.0 ns. For comparison with the solution structure of the RPSB, two additional simulations of 1.0 ns each were performed under the same conditions with the RPSB attached to an Ala-Lys-Thr peptide in a box of water, both in the 11-*cis* (SOLcis) and in the *all-trans* (SOLtrans) state.

pK_A Calculations. The intrinsic pK_A of the side chain of Glu181 was estimated in situ via numerical solution of the Poisson−Boltzmann equation (*55*−*57*) with the program Delphi (*32*, *33*). The change in electrostatic free energy associated with moving an isolated amino acid from aqueous solution to the protein environment was calculated for the protonated and the unprotonated form using dielectric constants of 80 for water and of 4 and 20 for the protein (*58*).

Data Analysis. Prior to data analysis, all rhodopsin snapshots were fitted to the corresponding X-ray structure, taking only the backbone of the TM helices (residues 34−64, 71−99, 107−135, 150−173, 200−229, 242−278, 288−309) as a reference. All root mean square displacements (RMSD) reported herein refer to heavy atoms only. The retinal binding pocket was defined by the 35 closest residues as described by Teller et al. (*31*). All molecular structures were drawn using VMD (*59*).

RESULTS AND DISCUSSION

The Protonation State of Glu181. Charged residues within the binding pocket can be expected to substantially influence the electronic structure and the overall properties of the chromophore. The X-ray data reveal that the side chain of Glu181, a residue of the second extracellular loop, is located close to the isomerizing C11−C12 bond (Figure 1b). The protonation state of Glu181 has not been established unequivocally by experiments, but it influences the properties of the photoreceptor as indicated by single point mutations. Mutants E181R, E181K, and E181P do not bind 11-*cis*-retinal to form a stable pigment, and E181Q displays a spectral red shift in the absence of sodium chloride, while other mutations do not alter the dark state absorption of the mutant pigments (*19*). The authors draw the conclusion that Glu181 is protonated in the dark state of rhodopsin. However, the absence of another protonated carboxylic acid band besides Asp83 and Glu122 in the vibrational spectra (*20*, *21*) of rhodopsin and bathorhodopsin suggests that Glu181 is negatively charged. Recent theoretical studies of the wavelength shift in short-wavelength cone opsins show that the calculations are extremely sensitive to the location of this residue (*15*).

Calculating the pK_A of ionizable groups in proteins is a nontrivial task, and several procedures have been proposed (*33*, *55*, *60*−*64*). Here, we use a combined approach, comparing results obtained by Poisson−Boltzmann calculations on the crystal structure to those coming from molecular dynamics simulations performed in both ionization states. Since the dielectric constant ϵ assumed for the protein turns out to be a crucial parameter in the Poisson−Boltzmann approach (*57*, *58*, *65*, *66*), we performed two sets of calculations using $\epsilon = 4$ and 20, respectively. Assuming a protein dielectric constant of 4, the calculated intrinsic pK_A of Glu181 is 13.0, indicating that the acid is protonated at pH 7. However, with a dielectric constant of 20, the intrinsic pK_A results to 4.3, and therefore the unprotonated form should be favorable under physiological conditions. These results thus do not establish the protonation state of Glu181 in an unambiguous way. We therefore performed MD simulations for both possible protonation states of Glu181 (simulations RHOp and RHO, respectively). These simulations supply clear evidence that the position of this residue in the X-ray structure is only stable in the unprotonated form. In simulation RHOp, the hydrogen-bonding network involving Glu181 disrupts after 630 ps of dynamics, and its side chain flips toward the aqueous interface (Figure 2a), thereby drastically increasing the distance between its carboxy group and the C11−C12 bond of the chromophore (Figure 2c). In the following, two internal water molecules (Wat1 and Wat2, Figure 2a,b) leave the binding pocket, probably due to less favorable interactions with some residues of the second extracellular loop. In contrast, the position of the charged Glu181 in the RHO simulation remains stable for the whole duration of the run of 7.0 ns, and the average distance between the carboxy group and the C11−C12 bond is essentially constant (6.2 ± 0.3 Å, Figure 2b,c). These results strongly indicate that Glu181 is most likely negatively charged.

Absolute Conformation of the Chromophore around the C12−C13 Bond. Due to steric interactions between the hydrogen bound to C10 and the C20 methyl group (Scheme 1), the polyene chain of the chromophore is not planar. Whereas the isolated retinal can adopt two chiral conformations in the C11−C12 region, NMR results indicate that the protein provides a tight binding pocket that is specific with respect to binding of one enantiomer only (*67*). The absolute conformation of the twist has been an issue in studying the molecular mechanism of the photoreaction because it is believed to influence the sense of rotation of the photoisomerization around the C11−C12 bond. Furthermore, it has been shown that the torsional twist induced by the C20 methyl group increases the quantum efficiency and accelerates the rate of the photoreaction (*68*).

Different experimental and theoretical studies provide controversial evidence about the helicity of the $\varphi_{C11-C12-C13-C14}$ dihedral angle. In the X-ray structure, the absolute sense of

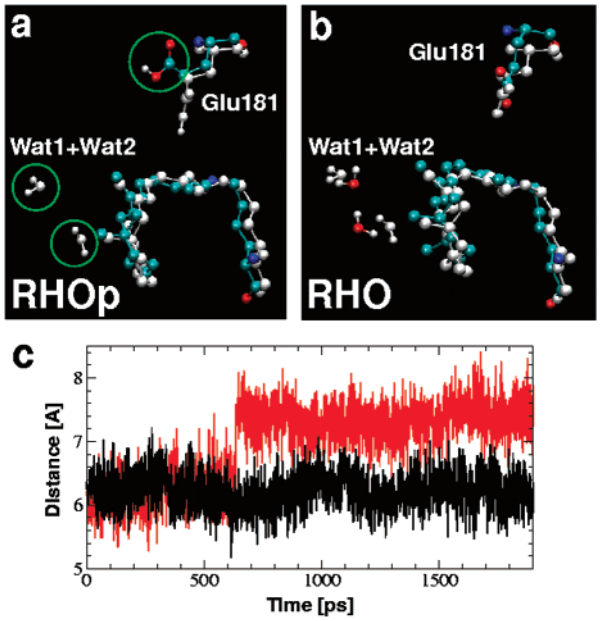

FIGURE 2: Comparison of the simulations RHOp and RHO (snapshots after 2.0 ns of MD) with the corresponding X-ray data. The crystal structure and the initially added internal water molecules (Wat1, Wat2) are shown in white. (a) RHOp (Glu181 protonated). Glu181 is turned away from the chromophore, and two water molecules left the binding pocket. (b) RHO (Glu181 negatively charged). Note that the initial structure is closely preserved. (c) Distance between the carboxyl oxygens of Glu181 and carbons C11 and C12 of the chromophore (RHOp, red line; RHO, black line) as a function of simulation time. The corresponding distance in the X-ray structure is 5.6 Å.

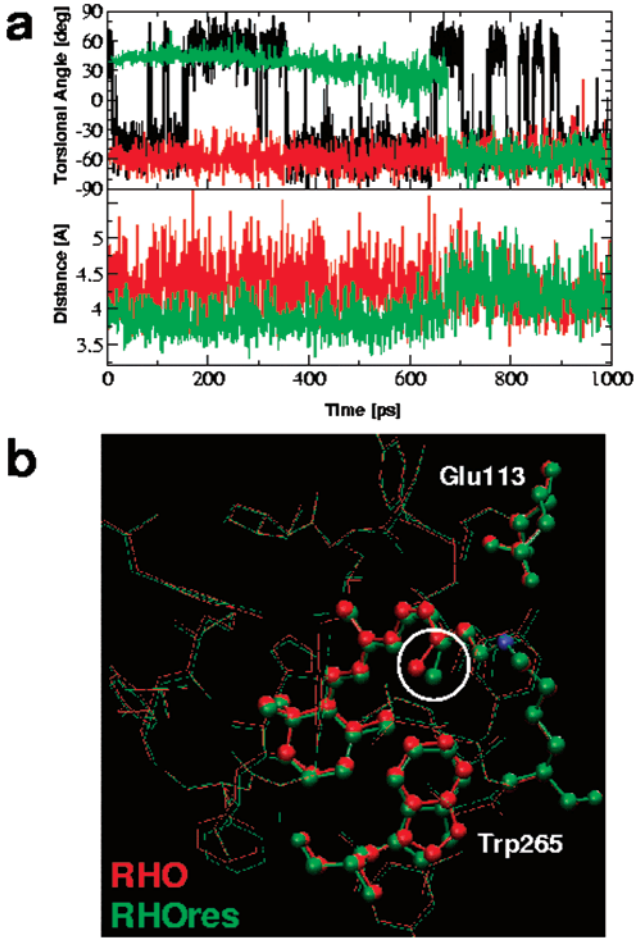

FIGURE 3: Study of the absolute conformation of the chromophore. (a) Top panel: $\varphi_{H-C10-C13-C20}$ of the chromophore in water (SOLcis, black line), in RHO (red line), and in RHOres (green line). Bottom panel: Distance between C20 and the closest carbon atom of Trp265. (b) Comparison of the average structures of simulations RHO (red) and RHOres (green), where the torsional angle $\varphi_{H-C10-C13-C20}$ is restrained to a positive value. The two structures differ only in the position of the C20 methyl group that comes into contact with Trp265 in RHOres.

twist around the C12−C13 single bond is *positive*.[3] This is in agreement with recent theoretical studies based on CD data (*25*−*27*), but it is at variance with results from solid-state NMR studies (*24*, *69*), CD spectra of rhodopsin with 11,12-dihydro chromophores (*28*), and studies with an 11,12-cyclopropyl RPSB (*29*). Here, we address the question of whether our model system shows a preference for either isomer or if it is compatible with both. For this purpose we set up two different simulations, one unrestrained (RHO) and one restraining the angle $\varphi_{H-C10-C13-C20}$ to a positive value (RHOres). Although the absolute values of the torsional angles will depend on the classical torsional parameters used for the chromophore, analogous simulations of bacteriorhodopsin have shown that the average conformation of the polyene chain does not depend strongly on the applied force field but is mainly determined by the arrangement of the binding pocket (*49*). A more sophisticated description of the chromophore would require a quantum chemical treatment within a QM/MM approach (*70*−*72*). However, the classical force field model used here can be expected to properly include the essential steric and electrostatic effects.

During the unrestrained MD simulation (RHO), $\varphi_{H-C10-C13-C20}$ remains always negative with a value of −57 ± 12° (Figure 3a, top panel, red line). In simulation RHOres, the system undergoes a MD simulation with the dihedral angle restrained to a value between +40° and +80° for as much as 675 ps, to allow the protein moiety to relax around this noncrystallographic chromophore conformation. Despite this long equilibration phase, the angle decreases when the restraining potential is weakened and changes immediately to a negative value upon releasing the restraint (Figure 3a, upper panel, green line). In contrast, the free 11-*cis* chromophore in solution (SOLcis) does not exhibit a preferred orientation, flipping several times between positive (+54 ± 15°) and negative (−54 ± 15°) values within the same time scale (Figure 3a, black line). During the restrained dynamics run, the C20 methyl group comes into van der Waals contact with Trp265 (Figure 3a, lower panel). This unfavorable interaction could be avoided by twisting the dihedral angle $\varphi_{C11-C12-C13-C14}$ to even more negative values. However, this is prevented by the constrained position of the bulky ionone ring on one hand and the orientation of the salt bridge between the Schiff base proton and Glu113 on the other. Comparison of the average structures of the binding pocket of RHO and RHOres shows almost complete agreement, except for the position of the C20 methyl group of the

[3] This corresponds to a clockwise rotation of the dihedral angle $\varphi_{C11-C12-C13-C14}$ (Scheme 1, solid line) or to a *negative* value of $\varphi_{H-C10-C13-C20}$ (Scheme 1, dashed line). The former is usually discussed in the literature, but since it is the latter dihedral angle that is directly influenced by the steric hindrance, we will in the following discussion mainly consider $\varphi_{H-C10-C13-C20}$. A positive value of $\varphi_{C11-C12-C13-C14}$ always corresponds to a negative value of $\varphi_{H-C10-C13-C20}$ and vice versa.

chromophore (Figure 3b). In summary, these results indicate that the binding pocket of the X-ray structure is only compatible with a positive dihedral angle $\varphi_{C11-C12-C13-C14}$ (corresponding to a negative value of $\varphi_{H-C10-C13-C20}$). The other isomer is not a stable equilibrium structure because it is strongly disfavored by the protein environment, in particular by the interactions with Trp265 and the salt bridge. This clear preference suggests that the photoisomerization of the C11−C12 bond is most likely to proceed via a clockwise rotation.

Characteristics of Rhodopsin with 11-cis-Retinal. Comparison of the simulations RHO1f88 and RHO, based on the two different refinements of the X-ray data (see Methods), showed that the more recent set of coordinates displays a significantly higher stability during our MD runs. The backbone RMSD of the binding pocket with respect to the crystal structure is 0.90 ± 0.06 Å in RHO1f88, nearly 50% larger than the one observed in RHO (0.62 ± 0.05 Å). On the basis of this observation, simulation RHO starting from PDB structure 1HZX (*31*) with a negatively charged Glu181 and a positive dihedral angle $\varphi_{C11-C12-C13-C14}$ seems to provide the best model for simulating the dark state of rhodopsin. During the simulated time of 7 ns, the system is stable, and the relative position in the membrane-mimicking environment is well preserved. The intrahelical hydrogen bond pattern of all seven TM helices as well as their overall packing is well maintained, the backbone RMSD from the X-ray structure being only 0.90 ± 0.08 Å. As can be expected, the loop regions and the carboxy-terminal tail on the other hand are very flexible, so that the overall backbone RMSD is significantly larger (RMSD 2.6 ± 0.3 Å).

The residues forming the binding pocket of the RPSB on the other hand are rather rigid (RMSD 0.62 ± 0.05 Å). The position of the retinal deviates little from the X-ray data (RMSD 0.48 ± 0.06 Å)[4] and shows only small fluctuations around its average structure (RMSD 0.25 ± 0.07 Å). The RPSB dynamics in solution differs from that in the protein by a distinctly higher fluctuation (RMSD 0.36 ± 0.10 Å), increased torsional flexibility of $\varphi_{H-C10-C13-C20}$ (see Figure 3a, upper panel), and a different dihedral angle $\varphi_{C5-C6-C7-C8}$ (SOLcis 12 ± 10° versus RHO −21 ± 9°). These findings clearly indicate that the protein environment imposes a pronounced rigidity and some strain on the retinal. The van der Waals contacts between the chromophore and the residues facing the binding pocket, in particular the steric interaction with Trp265, a highly conserved residue among visual pigments, are thus crucial for the stabilization of the retinal conformation in the dark state. This finding is in agreement with mutation studies of Trp265 that show that this residue plays an important role in retinal binding, reduction of the dark state activity, spectral tuning, and transducin activation (*73*, *74*).

A further issue of direct relevance to the photoisomerization process (*75*) is the nature of the structural interface between the chromophore and its counterion Glu113. FTIR difference spectra between rhodopsin and bathorhodopsin suggest that the interaction between the RPSB and the counterion Glu113 should be mediated by at least one water molecule (*76*). Solid-state NMR experiments further suggest the water-bridged distance between the counterion and the Schiff base nitrogen to be 4.3 ± 0.1 Å (*75*, *77*, *78*). However, in the X-ray structure there is not enough space for a water molecule (N−O distance 3.3 Å; see Scheme 1 for atom labeling), and instead a direct salt bridge is formed. This structural feature is maintained throughout our simulations, although one water molecule is always present close to the salt bridge, hydrogen bonded to Glu113, Thr94, and Ala117 (Wat3, Figure 1b).

The tertiary structure of the protein is stabilized via several interhelical hydrogen bonds. Four distinct hydrogen-bonding networks have been identified on the basis of the crystal structure (*9*), all of which remain stable during our simulations. In addition to the hydrogen bonds present in the X-ray model, we observe interhelical hydrogen bonds that connect, e.g., networks I (Asn55, Asp83, Gly120, Ala299) and IV (Met257, Asn302) with Trp265, Ser298, and Tyr301 through structured water molecules.[5] Most of these residues are highly conserved and have been shown to play an important role in the function of the photoreceptor (*9*, *73*, *79*, *80*). Other stable interhelical hydrogen bonds exist, e.g., between helices I and VII (Tyr43−Phe293), helices III and V (Asp122−His211), helices IV and V (Ala166−Tyr206), helices V and VI (Tyr223−Ile255), and helices VI and VII (Arg252−Met309). The interaction between helices V and VI is particularly interesting, because it is not present in the crystal structure, while one of the partaking residues (Tyr223) has been suggested to play an important role in signal transduction (*81*). On the extracellular side of the chromophore binding pocket, a network involving Glu181, Met183, Ser186, Cys187, Tyr191, Tyr 268, Thr 289, and water seems to be responsible for keeping Glu181 oriented toward the chromophore. The ten internal water molecules placed initially inside the protein keep their positions closely (average fluctuation 1.4 Å) and participate in all hydrogen-bonding networks.

Forcing the Chromophore from 11-cis to all-trans. The primary reaction in the rhodopsin photocycle, the *cis*−*trans* isomerization of the C11−C12 double bond of the chromophore, occurs in an electronically excited state on the subpicosecond time scale. A comprehensive description of this reaction requires a quantum mechanical treatment of the system in the excited state (see, e.g., refs *14*, *72*, and *82*−*90*). Here, we use instead a purely classical approach to enforce the isomerization process by applying a harmonic restraint to the $\varphi_{C10-C11-C12-C13}$ dihedral angle (Scheme 1). In this way, any explicit electronic effects are neglected, but we can obtain an idea of the main steric environment constraints that are imposed on the chromophore during and after the isomerization process. Considering the ultrafast time scale of the photoreaction (200 fs), which does not allow for large protein rearrangements to take place, one can indeed assume, as a first approximation, that the steric interactions between the chromophore and the rigid protein environment provide the main contribution to the trigger of the signal transduction pathway (*82*). To investigate the possible dynamics of the chromophore in the binding pocket immediately after isomerization, 24 simulations were carried

[4] However, the conformation around the Schiff base linkage resembles the one found in structures 1F88 and 1L9H, with the Schiff base proton pointing toward the counterion.

[5] A list of interhelical hydrogen bonds is available as Supporting Information.

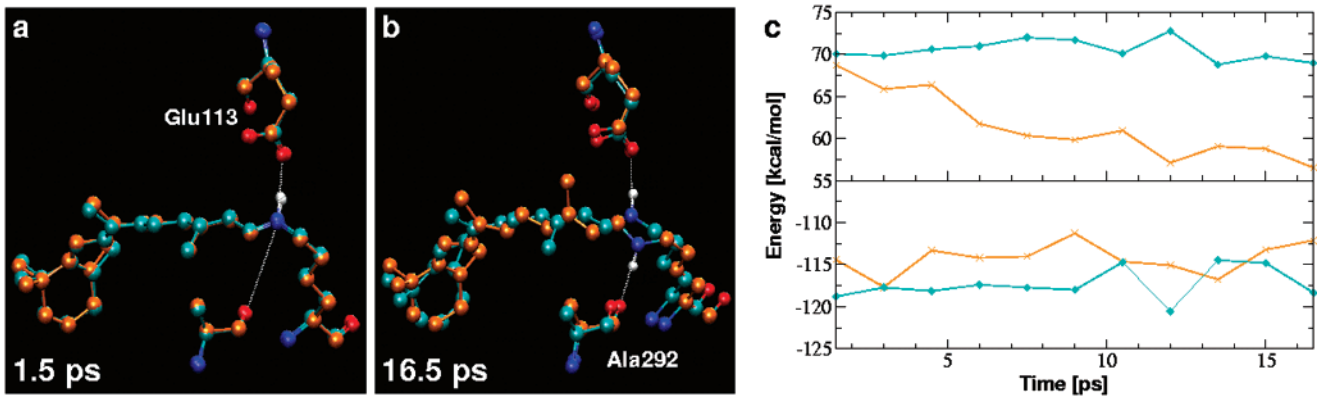

FIGURE 4: Isomerization pathways of the chromophore in the protein binding pocket explored by forcing the C11−C12 bond from *cis* to *trans*. In 50% of the 24 restrained isomerization dynamics (see Methods for details), the salt bridge is preserved (turquoise); in the other cases, it is broken (orange). Average structures of the two sets are reported after 1.5 ps (a) and after 16.5 ps (b) of dynamics. (c) Internal energy of the chromophore (top panel) and interaction energy of the chromophore with the binding pocket (bottom panel) during the unrestrained MD following the isomerization trials. For each set the energies are averaged over the 12 simulations.

out, where the C11−C12 double bond was forced to isomerize by applying a restraint to the dihedral angle $\varphi_{C10-C11-C12-C13}$, which was varied from −10° to 180° within 1.5 ps.[6] In agreement with our previous findings concerning the absolute orientation of the RPSB around the C12−C13 bond, we observe that clockwise rotation is clearly favored over counterclockwise twists.

For all trials, clockwise isomerization yields a very similar chromophore structure in which the salt bridge is conserved (Figure 4a) and the ionone ring has not moved significantly from its original position. These two positional constraints as well as the attachment to the protein backbone via Lys296 impose a very twisted conformation of the polyene chain directly after isomerization. This is clearly evident from the orientation of the C19 and C20 methyl groups ($\varphi_{C19-C9-C13-C20} = 70°$). Furthermore, all dihedral angles of the retinal are far from their minimum trans value of 180° (e.g., $\varphi_{C8-C9-C10-C11} = -153°$, $\varphi_{C12-C13-C14-C15} = -158°$).

After isomerization, we performed independent dynamics runs for each of the 24 trial simulations in which the systems evolved unrestrained for an additional 15 ps. The statistics of these dynamics reveal two different subsequent pathways as illustrated in Figure 4a,b. In 50% of the cases the salt bridge is preserved (turquoise), and in the remaining 50% it is disrupted (orange). In the latter class, the Schiff base proton forms a hydrogen bond with Ala292. The chromophore can adopt an almost planar geometry, resulting in a lowering of its internal energy (Figure 4c, upper panel). This stabilization effect is partly canceled out by a less favorable interaction energy with the environment (Figure 4c, lower panel). In the cases in which the salt bridge is preserved, the internal strain remains high, a fact that is clearly apparent from the preservation of the highly twisted state of the C19 and C20 methyl groups (Figure 4b, $\varphi_{C19-C9-C13-C20} = 70°$). This set of simulations is in better agreement with data that provides evidence that the salt bridge is not disrupted upon batho formation (*30*) and that bathorhodopsin adopts a highly twisted structure (*12*, *91*, *92*). Therefore, we will in the following refer only to the simulation set that preserves the relevant interaction with the counterion.

[6] To be able to account for the essential features of both the cis and the trans isomer, the force field has initially been optimized for both configurations (as described in Methods).

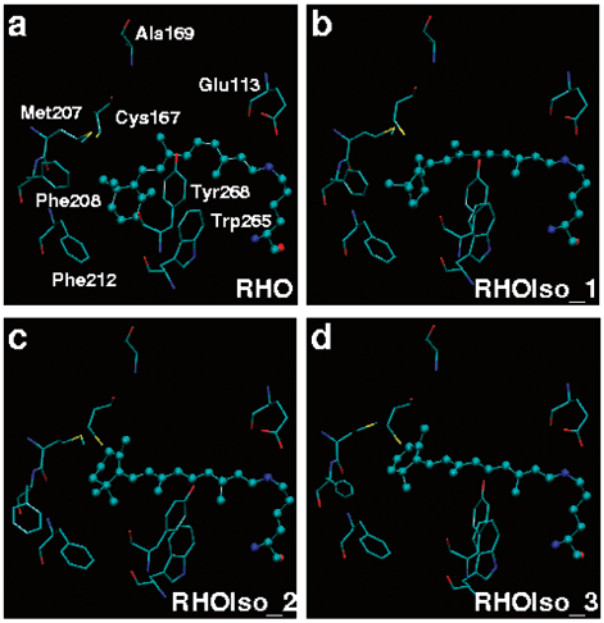

FIGURE 5: Average structures of the chromophore and surrounding residues mentioned in the text: (a) in the dark state (RHO); (b) after the isomerization (RHOiso_1, 0.6−2.1 ns); (c) after the flip of the ionone ring (RHOiso_2, 2.5−4.0 ns); (d) RHOiso_3 (5.0−6.5 ns).

Dynamics of Rhodopsin with all-trans-Retinal. One simulation (RHOiso) with an intact salt bridge was extended to the nanosecond time scale in order to investigate how the structural strain induced by the isomerization is propagated. Up to 1.65 ns after the isomerization, no significant changes take place in the chromophore and its direct environment. The geometry of the RPSB remains internally strained (RHOiso_1, Figure 5b, torsional parameters in Table 1), while the structure of the binding pocket is similar to the one in the dark state (RHO, Figure 5a). After 1.7 ns, internal strain of the chromophore is released by flipping the ionone ring toward helices IV and V and the second extracellular loop and away from helix VI (RHOiso_2, Figure 5c; for the helix numbering, see Figure 1a).[7] This leaves the chromophore in an essentially planar *all-trans* conformation with the polyene chain roughly parallel to the membrane

[7] A movie of this simulation is available as Supporting Information.

Table 1: Torsional Angles of the RPSB in Different Simulations[a]

torsional angle	RHO	SOLcis	RHOiso_1	RHOiso_2	RHOiso_3	SOLtrans
C4−C5−C6−C7	151 (11)	−141 (12)	108 (12)	157 (10)	150 (16)	−142 (12)
C5−C6−C7−C8	−21 (9)	12 (10)	−15 (10)	−18 (9)	−16 (12)	12 (10)
C6−C7−C8−C9	179 (5)	−179 (5)	−173 (5)	180 (5)	−178 (5)	180 (5)
C7−C8−C9−C10	172 (6)	−179 (7)	171 (6)	174 (7)	172 (6)	−179 (7)
C8−C9−C10−C11	176 (5)	179 (5)	−158 (5)	−174 (6)	−170 (5)	180 (5)
C9−C10−C11−C12	171 (6)	179 (7)	180 (6)	177 (7)	−179 (6)	180 (6)
C10−C11−C12−C13	−10 (5)	−2 (8)	−161 (6)	−172 (5)	−172 (5)	180 (5)
C11−C12−C13−C14	170 (5)	177 (10)	−171 (5)	−178 (6)	−175 (5)	180 (6)
C12−C13−C14−C15	176 (5)	180 (6)	−171 (5)	−179 (5)	−177 (5)	180 (6)
C13−C14−C15−N	178 (5)	180 (6)	−179 (5)	174 (5)	178 (5)	180 (6)
C14−C15−N-Lys	175 (5)	180 (5)	−173 (5)	−178 (5)	−178 (5)	180 (5)
H−C10−C13−C20	−58 (12)	−17 (51)	−125 (14)	−150 (18)	−146 (16)	180 (20)

[a] The average values and the root mean square deviations (in parentheses) are given in degrees. The atom numbering is given in Scheme 1. For the labels of the simulations, see text.

plane and the ionone ring extending in the same direction (Table 1). An inspection of the internal energy of the chromophore (Figure 6a, top panel) and its interaction energy with the environment (Figure 6a, bottom panel) shows that the 11-*cis* conformation (RHO, black line) has the lowest overall energy. After the isomerization, the internal energy of the retinal increases substantially (RHOiso_1, red line), while after the flip of the ionone ring, this internal stress is distributed to the interaction with the protein environment (RHOiso_2, green line).

As a consequence of the movement of the ionone ring, the binding pocket of the chromophore starts to rearrange substantially. Triggered by movement of Tyr268, the backbone of helix VI moves away from the chromophore, while the switch of the ionone ring pushes the side chains of Cys167, Met207, and Phe208 as well as two water molecules away (Wat1 and Wat2, Figure 1b). Further small conformational and orientational changes of the chromophore occur up to the end of the simulation of 7 ns (RHOiso_3, Figure 5d). They are induced by rearrangements of nearly all aromatic residues (Phe91, Tyr178, Tyr191, Phe203, Phe208, Phe212, Phe261, Trp265, Tyr268, Phe293) within the binding pocket.

In the overall protein structure, remarkable changes take place due to the rearrangement of the retinal. From the RMSD plot (Figure 6b) it is clearly visible that a conformational change takes place in the tertiary structure of the protein 1.75 ns after the isomerization (after 2.2 ns of the overall simulation time) and thus about 100 ps after the movement of the ionone ring. This structural rearrangement is mainly located in helix VI, more specifically in the extracellular half of it (residues 262−275) which moves away from the protein core. It is subsequently propagated to helices V and IV and results in a complex global movement of these helices. While the extracellular sides of helices V and VI move apart, the conformation of helix IV changes in the intracellular part.

The RHO and the RHOiso simulations differ also in some of the hydrogen-bonding patterns. In network I, there is an additional bond forming between Leu76 and Asn302 as a consequence of the movement of Asn302 away from helix VI. Helices I and VII form a bond between Tyr43 and Thr297 instead of Phe293. One hydrogen bond between helices IV and V (Ala166−Tyr206) is lost. Most changes occur as expected in the hydrogen bonding of helix VI. While around the chromophore pocket bonding is increased between Trp265, Ala295, and Ser298, the interactions with helices V (Tyr223−Ile255) and VII (Arg252−Met309) in the cytoplasmic region are lost.

In summary, there are two distinct regions of the protein in which hydrogen bond changes take place within a few nanoseconds after *cis*−*trans* isomerization. One is located around the retinal and involves breaking and forming of bonds between five helices (I, IV, V, VI, VII). The other is located at the cytoplasmic end of the TM portion of the protein and implies the rupture of two interhelical hydrogen bonds with helix VI (V−VI, VI−VII). This shows a propagation of the strain energy and is in accordance with the findings that the cytoplasmic end of helix VI moves for G-protein activation (*93*−*95*).

Only few experimental findings about the structural characteristics of the early photoproducts are currently available for the purpose of a direct comparison with the intermediates observed during our MD simulations. However, data provided by cross-linking experiments suggest that while in the dark state the ionone ring is exclusively linked to Trp265, in lumirhodopsin it is connected to Ala169 (helix IV) (*74*, *96*, *97*). This is a surprising result, since in the X-ray structure Ala169 points toward the membrane interface and is located 14 Å away from the ionone ring. Our MD simulations show that this distance decreases substantially upon isomerization and relocation of the ring (Figure 6c) and thus offer for the first time a possible rationale for this puzzling experimental observation. While the ionone ring is in contact with Cys167 in the dark state, Cys167 moves away after the flip, and the ring comes into contact with Ala168. A further move of the ring toward helix IV, or a small clockwise rotation of this helix (seen from the extracellular side), can bring Ala169 into direct contact with the chromophore.

SUMMARY AND CONCLUSIONS

We present molecular dynamics simulations of bovine rhodopsin in a membrane mimetic environment based on the recent crystal structure of the dark-adapted 11-*cis* form. These simulations demonstrate that (i) the active site geometry observed in the X-ray data is only maintained if Glu181, a residue close to the isomerizing bond, is negatively charged and (ii) the active site pocket is only compatible with a positive helical twist around the C12−C13 bond of the chromophore. Thus our simulations help to elucidate two

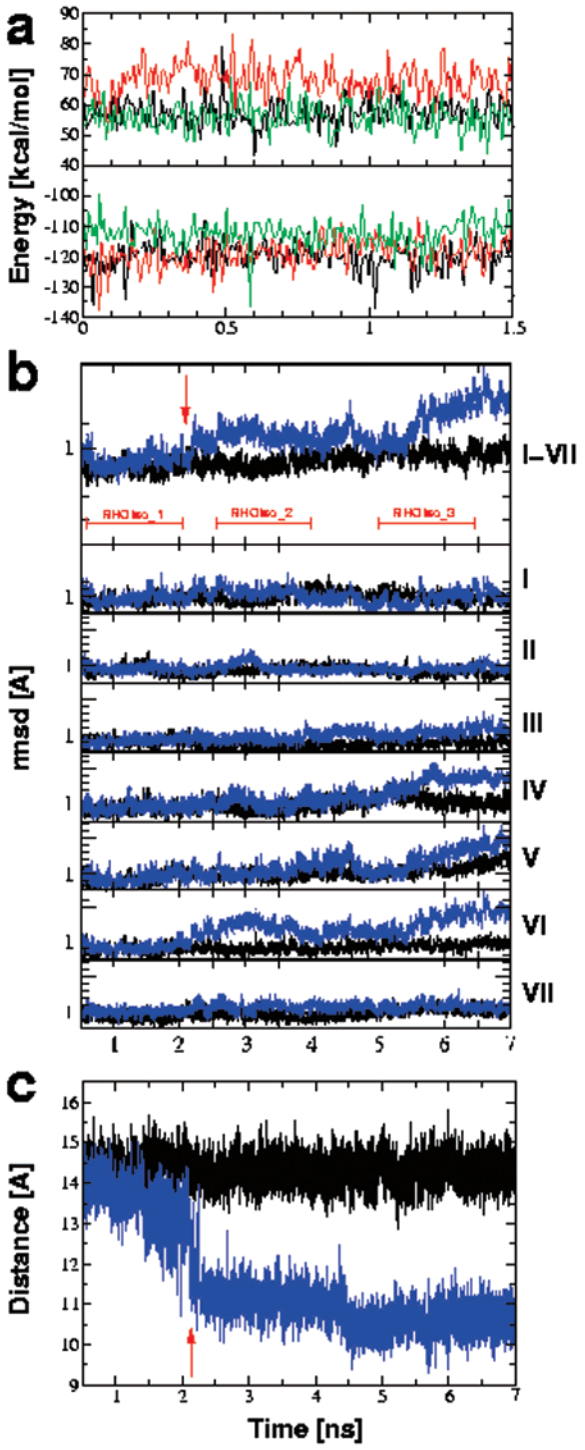

FIGURE 6: Comparison of the dynamics in the dark state (RHO) and in the isomerized state (RHOiso). (a) Internal energy (top panel) and interaction energy with the binding pocket (bottom panel) of the chromophore in RHO (black), RHOiso_1 (red), and RHOiso_2 (green). (b) Backbone RMSD of the TM helix bundle (top panel) and of the single helices (panels I−VII) as a function of the simulated time in RHO (black) and RHOiso (blue). (c) Distance between the ionone ring and Ala169 in RHO (black) and RHOiso (blue). The time when the ionone ring switches position in RHOiso is indicated by the red arrows.

controversial issues concerning the dark state that have a direct bearing on the isomerization process.

By performing a series of isomerization trials within the limits of a molecular mechanics description, we are able to generate a possible structural model for the photoisomerized *all-trans* form and to follow its relaxation during the first few nanoseconds. In particular, the simulations presented here allow us to study how the structural strain induced by isomerization is released and transmitted to the surrounding protein. According to our simulations, the number of initial relaxation routes is very limited. In the early steps of the signaling pathway, the highly localized structural perturbation caused by photoisomerization of the C11−C12 double bond is first mediated to the entire chromophore by inducing a narrowly defined highly strained, twisted and bent geometry. Our MD simulations suggest that the major pathway for strain release is a switch of the ionone ring that serves as a trigger for a propagation of the signal to the surrounding helical bundle. The complete structural rearrangements of the protein that lead to G-protein activation lie clearly outside our time window. Nonetheless, we are able to observe the onset of these changes that involve initial displacements of the residues in the binding pocket and subsequently a slow structural rearrangement of the helical bundle, in particular helix VI and to a lesser extent helices IV and V (see Figure 1a). In this way, the initial distortion of the chromophore is transmitted and amplified to larger and larger regions of the protein. Our simulations provide for the first time an atomistic picture of the early steps of the signaling pathway in rhodopsin as a prototypical G-protein-coupled receptor.

ACKNOWLEDGMENT

We thank R. E. Stenkamp and D. C. Teller for providing us with the structure of 1HZX prior to PDB release. G. Folkers and L. Scapozza are acknowledged for modeling unresolved parts of the protein with the simulation package SYBYL. We are grateful to I. Frank for motivating this study and to P. Carloni for many helpful discussions.

SUPPORTING INFORMATION AVAILABLE

Table 1 with the force field for the RPSB, Table 2 with selected interhelical hydrogen bonds from the crystal structure and from the simulations, and Movie 1 from the RHOiso simulation, showing the relocation of the ionone ring. This material is available free of charge via the Internet at http://pubs.acs.org.

REFERENCES

1. Ji, T. H., Grossmann, M., and Ji, I. (1998) *J. Biol. Chem. 273*, 17299−17302.
2. Gether, U., and Kobilka, B. K. (1998) *J. Biol. Chem. 273*, 17979−17982.
3. Marinissen, M. J., and Gutkind, J. S. (2001) *Trends Pharmacol. Sci. 22*, 368−376.
4. Flower, D. R. (1999) *Biochim. Biophys. Acta 1422*, 207−234.
5. Palczewski, K., Kumasaka, T., Hori, T., Behnke, C. A., Motoshima, H., Fox, B. A., Le Trong, I., Teller, D. C., Okada, T., Stenkamp, R. E., Yamamoto, M., and Miyano, M. (2000) *Science 289*, 739−745.
6. Hamm, H. E. (2001) *Proc. Natl. Acad. Sci. U.S.A. 98*, 4819−4821.
7. Meng, E. C., and Bourne, H. R. (2001) *Trends Pharmacol. Sci. 22*, 587−593.
8. Ebrey, T., and Koutalos, Y. (2001) *Prog. Retinal Eye Res. 20*, 49−94.
9. Menon, S. T., Han, M., and Sakmar, T. P. (2001) *Physiol. Rev. 81*, 1659−1688.
10. Okada, T., Ernst, O. P., Palczewski, K., and Hofmann, K. P. (2001) *Trends Biochem. Sci. 26*, 318−324.
11. Yoshizawa, T., and Wald, G. (1963) *Nature 197*, 1279−1285.

12. Palings, I., van den Berg, E. M., Lugtenburg, J., and Mathies, R. A. (1989) *Biochemistry 28*, 1498−1507.
13. Kliger, D. S., and Lewis, J. W. (1995) *Isr. J. Chem. 35*, 289−307.
14. Yamamoto, S., Wasada, H., Kakitani, T., and Yamato, T. (1999) *J. Mol. Struct. (THEOCHEM) 461*−*462*, 463−471.
15. Kusnetzow, A., Dukkipati, A., Babu, K. R., Singh, D., Vought, B. W., Knox, B. E., and Birge, R. R. (2001) *Biochemistry 40*, 7832−7844.
16. Sakmar, T. P., Franke, R. R., and Khorana, H. G. (1989) *Proc. Natl. Acad. Sci. U.S.A. 86*, 8309−8313.
17. Zhukovsky, E. A., and Oprian, D. D. (1989) *Science 246*, 928−930.
18. Fahmy, K., Jager, F., Beck, M., Zvyaga, T. A., Sakmar, T. P., and Siebert, F. (1993) *Proc. Natl. Acad. Sci. U.S.A. 90*, 10206−10210.
19. Yan, E. C., Kazmi, M. A., De, S., Chang, B. S., Seibert, C., Marin, E. P., Mathies, R. A., and Sakmar, T. P. (2002) *Biochemistry 41*, 3620−3627.
20. Nagata, T., Terakita, A., Kandori, H., Shichida, Y., and Maeda, A. (1998) *Biochemistry 37*, 17216−17222.
21. Kandori, H., Kinoshita, N., Yamazaki, Y., Maeda, A., Shichida, Y., Needleman, R., Lanyi, J. K., Bizounok, M., Herzfeld, J., Raap, J., and Lugtenburg, J. (1999) *Biochemistry 38*, 9676−9683.
22. Birge, R. R., Murray, L. P., Pierce, B. M., Akita, H., Balogh-Nair, V., Findsen, L. A., and Nakanishi, K. (1985) *Proc. Natl. Acad. Sci. U.S.A. 82*, 4117−4121.
23. Mollevanger, L. C., Kentgens, A. P., Pardoen, J. A., Courtin, J. M., Veeman, W. S., Lugtenburg, J., and De Grip, W. J. (1987) *Eur. J. Biochem. 163*, 9−14.
24. Han, M., and Smith, S. O. (1995) *Biochemistry 34*, 1425−1432.
25. Buss, V., Kolster, K., Terstegen, F., and Vahrenhorst, R. (1998) *Angew. Chem., Int. Ed. Engl. 37*, 1893−1895.
26. Buss, V. (2001) *Chirality 13*, 13−23.
27. Kampermann, H., Kolster, K., and Buss, V. (2001) *J. Mol. Model. 7*, 132−139.
28. Tan, Q., Lou, J., Borhan, B., Karnaukhova, E., Berova, N., and Nakanishi, K. (1997) *Angew. Chem., Int. Ed. Engl. 36*, 2089−2093.
29. Lou, J., Hashimoto, M., Berova, N., and Nakanishi, K. (1999) *Org. Lett. 1*, 51−54.
30. Pan, D., Ganim, Z., Kim, J. E., Verhoeven, M. A., Lugtenburg, J., and Mathies, R. A. (2002) *J. Am. Chem. Soc. 124*, 4857−4864.
31. Teller, D. C., Okada, T., Behnke, C. A., Palczewski, K., and Stenkamp, R. E. (2001) *Biochemistry 40*, 7761−7772.
32. Gilson, M. K., Sharp, K., and Honig, B. (1987) *J. Comput. Chem. 9*, 327−335.
33. Honig, B., and Nicholls, A. (1995) *Science 268*, 1144−1149.
34. Zhang, L., and Hermans, J. (1996) *Proteins 24*, 433−438.
35. Okada, T., Fujiyoshi, Y., Silow, M., Navarro, J., Landau, E. M., and Shichida, Y. (2002) *Proc. Natl. Acad. Sci. U.S.A. 99*, 5982−5987.
36. Moore, P. B., Zhong, Q., Husslein, T., and Klein, M. L. (1998) *FEBS Lett. 431*, 143−148.
37. Zhong, Q., Husslein, T., Moore, P. B., Newns, D. M., Pattnaik, P., and Klein, M. L. (1998) *FEBS Lett. 434*, 265−271.
38. Zhong, Q., Jiang, Q., Moore, P. B., Newns, D. M., and Klein, M. L. (1998) *Biophys. J. 74*, 3−10.
39. Guidoni, L., Torre, V., and Carloni, P. (1999) *Biochemistry 38*, 8599−8604.
40. Guidoni, L., Torre, V., and Carloni, P. (2000) *FEBS Lett. 477*, 37−42.
41. Unger, V. M., Hargrave, P. A., Baldwin, J. M., and Schertler, G. F. (1997) *Nature 389*, 203−206.
42. Wang, J., Cieplak, P., and Kollman, P. A. (2000) *J. Comput. Chem. 21*, 1049−1074.
43. Kaminski, G., Duffy, E. M., Matsui, T., and Jorgensen, W. L. (1994) *J. Phys. Chem. 98*, 13077−13082.
44. Chen, B., Martin, M. G., and Siepmann, J. I. (1998) *J. Phys. Chem. B 102*, 2578−2586.
45. Jorgensen, W. L., Chandrasekhar, J., Madura, J. D., Impey, R. W., and Klein, M. L. (1983) *J. Chem. Phys. 79*, 926−935.
46. Bayly, C. I., Cieplak, P., Cornell, W. D., and Kollman, P. A. (1993) *J. Phys. Chem. 97*, 10269−10280.
47. Cornell, W. D., Cieplak, P., Bayly, C. I., and Kollman, P. A. (1993) *J. Am. Chem. Soc. 115*, 9620−9631.
48. Frisch, M. J., Trucks, G. W., Schlegel, H. W., and Scuseria, G. E. (1998) *Gaussian 98*, Gaussian, Inc., Pittsburgh, PA.
49. Tajkhorshid, E., Baudry, J., Schulten, K., and Suhai, S. (2000) *Biophys. J. 78*, 683−693.
50. Tajkhorshid, E., Paizs, B., and Suhai, S. (1999) *J. Phys. Chem. B 103*, 4518−4527.
51. Pearlman, D. A., Caldwell, J. W., Cheatham, T. E. I., Ross, W. S., Simmerling, C., Darden, T., Merz, K. M., Stanton, R. V., Chen, A., Vincent, J. J., Crowley, M., Tsui, V., Radmer, R., Duan, Y., Pitera, J., Massova, I., Seibel, G. L., Singh, U. C., Weiner, P., and Kollmann, P. A. (2000) *AMBER [6.0]*, University of California, San Francisco.
52. Essman, U., Perera, L., Berkowitz, M. L., Darden, T. A., Lee, H., and Pedersen, L. G. (1995) *J. Chem. Phys. 103*, 8577−8593.
53. Ryckaert, J. P., Ciccotti, G., and Berendsen, H. J. C. (1977) *J. Comput. Chem. 23*, 327−341.
54. Berendsen, H. J. C., Postma, J. P. M., Van Gunsteren, W. F., DiNola, A., and Haak, J. R. (1984) *J. Chem. Phys. 81*, 3684−3690.
55. Bashford, D., and Karplus, M. (1990) *Biochemistry 29*, 10219−10225.
56. Yang, A. S., Gunner, M. R., Sampogna, R., Sharp, K., and Honig, B. (1993) *Proteins 15*, 252−265.
57. Schutz, C. N., and Warshel, A. (2001) *Proteins 44*, 400−417.
58. Antosiewicz, J., McCammon, J. A., and Gilson, M. K. (1996) *Biochemistry 35*, 7819−7833.
59. Humphrey, W., Dalke, A., and Schulten, K. (1996) *J. Mol. Graphics 14*, 33−38.
60. Warshel, A. (1981) *Biochemistry 20*, 3167−3177.
61. Warshel, A., and Russell, S. T. (1984) *Q. Rev. Biophys. 17*, 283−422.
62. Kollman, P. A. (1993) *Chem. Rev. 93*, 2395−2417.
63. Sham, Y. Y., Chu, Z. T., and Warshel, A. (1997) *J. Phys. Chem. B 101*, 4458−4472.
64. Warshel, A., and Papazyan, A. (1998) *Curr. Opin. Struct. Biol. 8*, 211−217.
65. Gilson, M. K., and Honig, B. H. (1986) *Biopolymers 25*, 2097−2119.
66. King, G., Lee, F. S., and Warshel, A. (1991) *J. Chem. Phys. 95*, 4366−4377.
67. Verdegem, P. J., Bovee-Geurts, P. H., De Grip, W. J., Lugtenburg, J., and de Groot, H. J. (1999) *Biochemistry 38*, 11316−11324.
68. Kochendoerfer, G. G., Verdegem, P. J., van der Hoef, I., Lugtenburg, J., and Mathies, R. A. (1996) *Biochemistry 35*, 16230−16240.
69. Han, M., and Smith, S. O. (1995) *Biophys. Chem. 56*, 23−29.
70. Hayashi, S., and Ohmine, I. (2000) *J. Phys. Chem. B 104*, 10678−10691.
71. Houjou, H., Inoue, Y., and Sakurai, M. (2001) *J. Phys. Chem. B 105*, 867−879.
72. Warshel, A., and Chu, Z. T. (2001) *J. Phys. Chem. B 105*, 9857−9871.
73. Nakayama, T. A., and Khorana, H. G. (1991) *J. Biol. Chem. 266*, 4269−4275.
74. Borhan, B., Souto, M. L., Imai, H., Shichida, Y., and Nakanishi, K. (2000) *Science 288*, 2209−2212.
75. Verhoeven, M. A., Creemers, A. F., Bovee-Geurts, P. H., De Grip, W. J., Lugtenburg, J., and de Groot, H. J. (2001) *Biochemistry 40*, 3282−3288.
76. Nagata, T., Terakita, A., Kandori, H., Kojima, D., Shichida, Y., and Maeda, A. (1997) *Biochemistry 36*, 6164−6170.
77. Creemers, A. F., Klaassen, C. H., Bovee-Geurts, P. H., Kelle, R., Kragl, U., Raap, J., De Grip, W. J., Lugtenburg, J., and de Groot, H. J. (1999) *Biochemistry 38*, 7195−7199.
78. Eilers, M., Reeves, P. J., Ying, W., Khorana, H. G., and Smith, S. O. (1999) *Proc. Natl. Acad. Sci. U.S.A. 96*, 487−492.
79. Le Gouill, C., Parent, J. L., Rola-Pleszczynski, M., and Stankova, J. (1997) *J. Biol. Chem. 272*, 21289−21295.
80. Han, M., Smith, S. O., and Sakmar, T. P. (1998) *Biochemistry 37*, 8253−8261.
81. Pogozheva, I. D., Lomize, A. L., and Mosberg, H. I. (1997) *Biophys. J. 72*, 1963−1985.
82. Warshel, A. (1976) *Nature 260*, 679−683.
83. Ben Nun, M., Molnar, F., Lu, H., Phillips, J. C., Martinez, T. J., and Schulten, K. (1998) *Faraday Discuss.*, 447−462.
84. Humphrey, W., Lu, H., Logunov, I., Werner, H. J., and Schulten, K. (1998) *Biophys. J. 75*, 1689−1699.
85. La Penna, G., Buda, F., Bifone, A., and de Groot, H. J. M. (1998) *Chem. Phys. Lett. 294*, 447−453.
86. Molteni, C., Frank, I., and Parrinello, M. (1999) *J. Am. Chem. Soc. 121*, 12177−12183.

87. Molnar, F., Ben Nun, M., Martinez, T. J., and Schulten, K. (2000) *J. Mol. Struct. (THEOCHEM) 506*, 169−178.
88. Gonzalez-Luque, R., Garavelli, M., Bernardi, F., Merchan, M., Robb, M. A., and Olivucci, M. (2000) *Proc. Natl. Acad. Sci. U.S.A. 97*, 9379−9384.
89. Warshel, A., and Parson, W. W. (2001) *Q. Rev. Biophys. 34*, 563−679.
90. Ben Nun, M., Molnar, F., Schulten, K., and Martinez, T. J. (2002) *Proc. Natl. Acad. Sci. U.S.A. 99*, 1769−1773.
91. Warshel, A., and Barboy, N. (1982) *J. Am. Chem. Soc. 104*, 1469−1476.
92. Eyring, G., Curry, B., Broek, A., Lugtenburg, J., and Mathies, R. (1982) *Biochemistry 21*, 384−393.
93. Farrens, D. L., Altenbach, C., Yang, K., Hubbell, W. L., and Khorana, H. G. (1996) *Science 274*, 768−770.
94. Dunham, T. D., and Farrens, D. L. (1999) *J. Biol. Chem. 274*, 1683−1690.
95. Cai, K., Klein-Seetharaman, J., Hwa, J., Hubbell, W. L., and Khorana, H. G. (1999) *Biochemistry 38*, 12893−12898.
96. Souto, M. L., Um, J., Borhan, B., and Nakanishi, K. (2000) *Helv. Chim. Acta 83*, 2617−2628.
97. Nakanishi, K. (2000) *Chem. Pharm. Bull. (Tokyo) 48*, 1399−1409.

BI026011H